Earth and Planetary Science Letters 295 (2010) 241–250

Contents lists available at ScienceDirect

Earth and Planetary Science Letters

journal homepage: www.elsevier.com/locate/epsl

Iron isotope fractionation between aqueous ferrous iron and goethite

Brian L. Beard [a,b,*], Robert M. Handler [c], Michelle M. Scherer [c], Lingling Wu [a,b], Andrew D. Czaja [a,b], Adriana Heimann [a,b,1], Clark M. Johnson [a,b]

[a] University of Wisconsin-Madison, Department of Geology and Geophysics, 1215 West Dayton Street, Madison WI 53706, United States
[b] NASA Astrobiology Institute, United States
[c] University of Iowa, Department of Civil and Environmental Engineering, 4105 Seamans Center, Iowa City, IA 52242, United States

ARTICLE INFO

Article history:
Received 21 January 2010
Received in revised form 31 March 2010
Accepted 1 April 2010
Available online 10 May 2010

Editor: R.W. Carlson

Keywords:
Fe isotopes
goethite
isotope fractionation
nanoparticles
fluid mineral fractionation

ABSTRACT

The equilibrium Fe isotope fractionation factor between aqueous Fe(II) and goethite has been experimentally measured to be -1.05 ± 0.08‰ in $^{56}Fe/^{54}Fe$ (2σ) at 22 °C, using the three-isotope method. Experiments were done using two sizes of goethite (81×11 nm and 590×42 nm), and the experimental products were subjected to serial extraction using acid partial dissolution techniques to determine if surface Fe(III) atoms have different isotopic properties than the bulk goethite. These experiments indicate that the interaction of $Fe(II)_{aq}$ and goethite is dynamic and results in complete or near-complete Fe isotope exchange over 30 days, involving at least four components: $Fe(II)_{aq}$, goethite, sorbed Fe(II), and $Fe(III)_{surface}$. The equilibrium fractionation factor between $Fe(II)_{aq}$ and $Fe(II)_{sorb}$ is the same for both sizes of goethite, at $\Delta^{56}Fe_{Fe(II)aq-Fe(II)sorb}=-1.24\pm0.14$‰; this fractionation factor is significantly different than the results of previous studies on Fe(II) sorption to goethite. The proportion of the $Fe(III)_{surface}$ component is greatest in the experiments that used the smallest goethite, and the $Fe(III)_{surface}$–$Fe(II)_{aq}$ fractionation is estimated to be at least +2.1‰. The high $Fe(III)_{surface}$–$Fe(II)_{aq}$ fractionation may exert a significant influence on the Fe isotope compositions of aqueous Fe(II) in natural systems that contain nanoparticulate goethite, including those involving bacterial iron reduction. These results demonstrate that the isotopic properties of nano-scale minerals may be distinct from micron-scale or larger minerals, as is the case for other thermodynamic properties of nanoparticles.

1. Introduction

The interaction of aqueous Fe(II) ($Fe(II)_{aq}$) with iron oxides and hydroxides is a dynamic process that produces a variety of reactions including: 1) sorption of $Fe(II)_{aq}$ onto the oxide surface, 2) exchange of electrons between Fe(II) and Fe(III), 3) loss of Fe(II) to the iron oxide via transport of electrons in the substrate, 4) production of more stable oxides through phase transformation, and 5) coupled electron and atom exchange (e.g., Cwiertny et al., 2008; Gorski and Scherer, 2009; Hansel et al., 2005; Larese-Casanova and Scherer, 2007; Pedersen et al., 2005; Silvester et al., 2005; Williams and Scherer, 2004; Yanina and Rosso, 2008). Of the crystalline iron oxide/hydroxides that occur in nature, goethite is the most common in lacustrine and marine sediments (e.g. van der Zee et al., 2003). There have been a number of Fe isotope studies that have investigated the reaction between $Fe(II)_{aq}$ and goethite, including studies of mass-dependent, "natural" isotopic fractionations by Icopini et al. (2004), Crosby et al.(2007), Jang et al. (2008), and Mikutta et al. (2009), as well as studies that have evaluated isotope exchange using enriched ^{55}Fe measured by alpha counting (Pedersen et al., 2005), and ^{57}Fe and ^{56}Fe isotope tracers measured by either Mössbauer spectroscopy or isotope ratio mass spectrometry (e.g., Handler et al., 2009; Silvester et al., 2005; Williams and Scherer, 2004). Collectively, these studies highlight the reactive nature of $Fe(II)_{aq}$–goethite interactions, and Handler et al. (2009) proposed that dynamic dissolution/re-precipitation may occur via a "redox-driven conveyor belt".

Studies of the naturally occurring, mass-dependent Fe isotope fractionations produced by $Fe(II)_{aq}$–goethite interactions have yielded a wide variety of results. Crosby et al. (2005, 2007) studied Fe isotope fractionation associated with $Fe(II)_{aq}$ produced by dissimilatory iron reducing (DIR) bacteria grown on goethite, and concluded that Fe isotope fractionation was largely driven by electron and atom exchange between $Fe(II)_{aq}$ and a reactive ferric layer ($Fe(III)_{reac}$) produced on the goethite surface. These reactions produced $Fe(II)_{aq}$ of low $\delta^{56}Fe$ value as compared to a higher $\delta^{56}Fe$ value for the reactive ferric layer. These studies also investigated the isotopic fractionations between $Fe(II)_{aq}$ and sorbed Fe(II) ($Fe(II)_{sorb}$), which Crosby et al. (2005, 2007) estimated to be ~-0.9‰ in $^{56}Fe/^{54}Fe$. Although the effects of sorption on the isotopic compositions of $Fe(II)_{aq}$ were significant during the initial stages of DIR, the effects became very small upon greater extents of reduction. In contrast, studies by Icopini

* Corresponding author. University of Wisconsin-Madison, Department of Geology and Geophysics, 1215 West Dayton Street, Madison WI 53706, United States. Tel.: +1 608 262 1806.
E-mail address: beardb@geology.wisc.edu (B.L. Beard).
[1] Current address: East Carolina University, Department of Geological Sciences, United States.

0012-821X/$ – see front matter © 2010 Elsevier B.V. All rights reserved.
doi:10.1016/j.epsl.2010.04.006

et al. (2004) and Jang et al. (2008) suggest that the Fe isotope variations associated with interaction of $Fe(II)_{aq}$ and goethite are largely controlled by sorption of Fe(II) onto goethite. Jang et al. (2008) proposed that in addition to sorption of Fe that had high $^{56}Fe/^{54}Fe$ ratios, there is a kinetic fractionation associated with electron transfer into the goethite structure that produces a ferrous material with a $^{56}Fe/^{54}Fe$ ratio that is higher than that of aqueous Fe. These conclusions were based on abiologic experiments (Icopini et al., 2004; Jang et al., 2008) and biological experiments in which aqueous Fe was produced by DIR bacteria grown on goethite (Icopini et al., 2004). Icopini et al. (2004) estimated there to be a 2.7 to 3.7‰ fractionation in $^{56}Fe/^{54}Fe$ between $Fe(II)_{sorb}$ and $Fe(II)_{aq}$, although this study did not measure the sorbed Fe component directly. Jang et al. (2008), using a similar approach to that of Icopini et al. (2004), estimated the fractionation between $Fe(II)_{sorb}$ and $Fe(II)_{aq}$ to be +0.29 to +2.30‰. In addition, Jang et al. (2008) calculated an "included" Fe(II) component in goethite (an Fe(II) component not released by 0.5 M HCl extraction) that initially had a $\delta^{56}Fe$ value that matched $Fe(II)_{aq}$, and with time became more similar to the $Fe(II)_{sorb}$ component. Because, however, the experimental protocols involved analysis of mixtures of $Fe(II)_{aq}$ and goethite, without partial dissolution of the solids or extraction of the sorbed component, it is difficult to reconcile these results with those of Crosby et al. (2005, 2007).

The Fe isotope fractionations produced during flow-through experiments that involved $Fe(II)_{aq}$ pumped through goethite-coated sand were reported by Mikutta et al. (2009). This study interpreted the observed fractionations to reflect sorption of Fe(II) coupled with minor atom exchange between $Fe(II)_{aq}$ and goethite, and Mikutta et al. (2009) estimated the equilibrium Fe isotope fractionation between $Fe(II)_{aq}$ and $Fe(II)_{sorb}$ to be −0.73‰ in $^{56}Fe/^{54}Fe$. This conclusion was based on assuming that the Fe isotope composition of the exchanged Fe is equal to the Fe isotope composition of $Fe(II)_{sorb}$, and, based on mass-balance modeling, it was estimated that ~3% of the exchangeable Fe pool experienced atom exchange.

The results of the Fe isotope studies of $Fe(II)_{aq}$–goethite interactions discussed above are difficult to apply to natural systems because of the wide variety of experimental approaches, and the fact that the equilibrium $Fe(II)_{aq}$–$Fe(II)_{sorb}$ and $Fe(II)_{aq}$–goethite Fe isotope fractionation factors have not been rigorously determined, which are required to understand potential kinetic effects. Here we apply the three-isotope method, using an enriched ^{57}Fe tracer, to constrain the extent of atom exchange between different components in the system $Fe(II)_{aq}$–goethite at room temperature. Through stepwise partial dissolution, the components that were open to isotopic exchange can be identified, including aqueous Fe(II), sorbed Fe(II), surface Fe(III), and bulk goethite. These results provide the most rigorous determination to date of equilibrium Fe isotope fractionation factors in fluid–mineral systems at low temperature, and when compared to fractionation factors calculated from theory, highlight important inconsistencies that need to be addressed.

2. Experimental design and analytical methods

2.1. Experimental setup

The experimental design is based on reacting aqueous ferrous ^{57}Fe-enriched solutions with goethite over 30 days. All experiments were performed in an anoxic glove box, and extreme care was taken to exclude O_2 from the experiments during sample extractions. All experiments were run at room temperature, which was stable at 22 ± 1 °C over the course of the experiments. Two types of goethite were investigated: 1) nanorod goethite that was 81 nm by 11 nm in dimension, and 2) microrod goethite that was 590 nm by 42 nm in dimension. The BET surface areas of the nanorod and microrod goethite were 110 and 40 m^2/g, respectively. Preparation of goethite and its mineralogical and morphological characterization is described in Cwiertny et al. (2008). The details of the experimental setup and the preparation of the aqueous ^{57}Fe-enriched solution that was reacted with goethite are described in Handler et al. (2009). Separate reactors were sacrificed for each time point, which avoids the changing mass-balance relations that would occur by serially sampling a single reactor for every time point. Each reactor contained 30 ± 0.3 mg of goethite, ~14.8 mL of a ~1 mM Fe(II) solution with 25 mM KBr, 25 mM HEPES, and the pH was adjusted to 7.5 by addition of small volumes of 0.5 mM KOH. There is some uncertainty in the solution volume of each reactor; this is due to variable solution retention on the 0.2 μm filters used to exclude solid ferric oxides formed by addition of the concentrated ferrous Fe solution to the HEPES-buffered solution, prior to introduction into the reactors. Replicate filtration of solutions showed that the average delivery volume of a 15 mL aliquot filtered through a 0.2 μm syringe filter was 14.8 ± 0.1 mL. The Fe concentration delivered to each bottle was also variable, reflecting differences in the delivered volumes of the concentrated stock ^{57}Fe-enriched solution into the HEPES-buffered solution. The starting Fe concentration in each reactor was measured via spectrophotometry, and ranged from 1.011 to 1.113 mM Fe(II). Every time point was duplicated or triplicated, which resulted in a total of 40 reactors for the micro and nanorod experiments that were sampled after 0.17, 12, 38, 74, 142, 354, and 717 h of $Fe(II)_{aq}$–goethite reaction. In addition, 4 control reactors of the aqueous Fe(II) solution without goethite were processed along with 2 controls each of micro and nanorod goethite that were exposed to an Fe-free buffer solution, respectively. These controls demonstrate that there was no oxidation of aqueous Fe(II) by O_2, and that the goethite did not dissolve or react in the Fe-free buffered solutions.

Five samples were taken from each reactor under anaerobic conditions. An aqueous Fe sample was collected by centrifugation, followed by decanting the solution and filtration. Following centrifugation, the solids were subjected to four serial partial dissolutions. The solution obtained from each partial dissolution was collected by centrifugation and decanting, followed by filtration using a 0.2 μm syringe filter. Extract 1 was a resuspension of the solids in 5 mL of 0.4 M HCl. Extract 2 consisted of a 45 minute resuspension in 60 °C HCl; the nanorods were subjected to a 1 M HCl solution, and the microrods to a 1.75 M HCl solution. Extract 3 was a repeat of extract 2, and extract 4 was complete dissolution of the remaining solids using 5 M HCl at 60 °C. The conditions used for extracts 1, 2, and 3 were optimized based on extensive testing so that extract 1 contained the maximum possible proportion of Fe(II), and extracts 2 and 3 contained the maximum possible proportion of Fe(III). Each sample was analyzed for its Fe isotope composition and Fe(II) and total Fe concentration. The protocols for total Fe and Fe(II) concentration analysis are given in Handler et al. (2009). The Fe abundances and speciation are reported in Supplementary information Table S1.

2.2. Fe isotope data presentation and analysis

Iron isotope compositions are described using standard δ notation, in units of per mil (‰):

$$\delta^{56}Fe = \left(^{56}Fe/^{54}Fe_{sample}/^{56}Fe/^{54}Fe_{standard} - 1\right)*10^3 \quad (1)$$

and

$$\delta^{57}Fe/^{56}Fe = \left(^{57}Fe/^{56}Fe_{sample}/^{57}Fe/^{56}Fe_{standard} - 1\right)*10^3 \quad (2)$$

Where the $^{56}Fe/^{54}Fe_{standard}$ and $^{57}Fe/^{56}Fe_{standard}$ are the average of igneous rocks (Beard et al., 2003). Note we use the term $\delta^{57}Fe/^{56}Fe$ rather than $\delta^{57}Fe$, because the later is commonly defined in the

literature based on $^{57}Fe/^{54}Fe$ ratios. The isotopic fractionation between two phases is defined as

$$\alpha^{56}_{A-B} = (^{56}Fe/^{54}Fe)_A/(^{56}Fe/^{54}Fe)_B \quad (3)$$

following standard practice, and an analogous definition may be based on $^{57}Fe/^{56}Fe$ ratios. To a very good approximation,

$$10^3 \ln\alpha^{56}_{A-B} \sim \Delta^{56}Fe_{A-B} = \delta^{56}Fe_A - \delta^{56}Fe_B \quad (4)$$

In general we focus in this study on the $^{56}Fe/^{54}Fe$ variations to infer equilibrium mass-fractionation factors because the starting materials had "normal" $^{56}Fe/^{54}Fe$ ratios; the extent of isotopic exchange is best monitored using the $^{57}Fe/^{56}Fe$ ratios because an enriched ^{57}Fe aqueous Fe(II) solution was used. If 100% isotopic exchange occurred, $^{57}Fe/^{56}Fe$ and $^{56}Fe/^{54}Fe$ ratios will provide the same information regarding mass-dependent isotopic fractionation factors, as discussed in more detail in Section 4.

Prior to isotopic analysis, all samples were purified using anion-exchange resin and HCl, following the methods of Beard et al. (2003). Ion-exchange column yields were determined using *Ferrozoine*, and were between 97 and 103%. The purified Fe was analyzed for its $^{56}Fe/^{54}Fe$ and $^{57}Fe/^{56}Fe$ isotope ratios using a Micromass *IsoProbe*. The measured Fe isotope composition of the IRMM-014 Fe isotope standard was $\delta^{56}Fe = -0.09 \pm 0.04$ and $\delta^{57}Fe/^{56}Fe = -0.03 \pm 0.05‰$ (average and 1-standard deviation of 4 analyses). Based on replicate analyses of standards and samples processed through the entire analytical procedure the $\delta^{56}Fe$ values are accurate and precise to 0.05‰ (1σ) and the accuracy and precision of the $\delta^{57}Fe/^{56}Fe$ values is slightly poorer, at 0.13‰ (1σ). Details of the analytical methods and the measured Fe isotope compositions are reported in Supplementary information Table S2.

2.3. Three-isotope method

The three-isotope method was employed to rigorously document the isotopic fractionation factor that would be achieved at complete isotope exchange, and thus likely represent the equilibrium isotope fractionation factor. This technique was initially developed by Matsuhisa et al. (1978) to study O isotope fractionation and has been employed for a variety of experimental studies for O (e.g., Matthews et al., 1983) and Fe (e.g., Shahar et al., 2008). This technique follows the isotope exchange between two components that do not initially plot upon the same mass-dependent isotope fractionation line because one component contains an enriched isotope relative to the other component. At complete isotopic exchange, the two components will plot along a common "secondary" mass-fractionation line which must pass through the isotopic composition of the system, as dictated by mass-balance. The difference in isotopic composition between the components that lie on the "secondary" mass-fractionation line is the isotopic fractionation factor. The true utility of this system is that in the case of simple two-component exchange that does not go to completion, it is possible to extrapolate to the isotopic composition at complete exchange. In cases where there are more than two components involved in incomplete isotope exchange it will be more difficult to extrapolate to conditions of complete exchange because the exchange trajectories defined by the components may be curves rather than lines.

3. Results

Addition of $Fe(II)_{aq}$ to goethite resulted in a rapid (<1 h) decrease in the aqueous Fe(II) concentration, reflecting sorption of Fe(II) to the goethite surface. Steady-state conditions with respect to net mass transport of Fe(II) were generally reached by ~200 h (Fig. 1), and this was reflected in the relatively constant Fe molar proportions results obtained for all experiments for time points ≥200 h, including the proportion of total Fe and the ferrous to total Fe ratio in all extracts for the micro and nanorod experiments (Fig 1, Table S1). The aqueous Fe and extract 1 in the nano and microrod experiments predominately consisted of ferrous Fe (>92% Fe(II) of total Fe), whereas extracts 2 and 3 were mostly ferric iron (Fig 1, Table S1). Extract 1 is therefore interpreted to reflect sorbed Fe(II), whereas extracts 2 and 3 reflect partial dissolution of surface goethite that underwent isotopic exchange (and possibly some unexchanged goethite), in addition to minor carryover of sorbed Fe(II) not removed by extract 1.

There are differences in the relative Fe proportions in the extracts between the nano and microrod experiments, where the nanorod experiments have the lower molar proportion of aqueous Fe and extract 4 as compared to the microrod experiments (Fig 1). Differences in the total Fe molar proportions between the micro and nanorod experiments are most likely a result of the differences in surface area. These differences in molar proportions are not an analytical artifact because the ratio of total Fe recovered from all extractions, relative to the known amount of Fe added to the reactors, is the same: 0.92 ± 0.07 and 0.93 ± 0.05, respectively.

Total Fe(II) recovery (sum of Fe(II) in the aqueous samples and all extracts) was achieved for the nanorod experiments. In contrast, Fe (II) recovery was incomplete for the longer duration microrod experiments, where there was typically a 4% loss in the amount of Fe(II) recovered. This loss of Fe(II) was unlikely to be caused by oxidation by O_2 because the nanorod experiments, which were treated identically to the microrod experiments, did not show such a phenomenon. A likely reason for this apparent Fe(II) loss in the microrod experiments is that these products did not pelletize as well as in the nanorod experiments during centrifugation, resulting in some loss of goethite and attendant loss of $Fe(II)_{sorb}$. Alternatively, loss of Fe(II) from the aqueous and sorbed Fe(II) pools to the ferric oxide in Fe(II)-iron oxide experiments has been observed in other Fe (II)-oxide experiments, and has been interpreted to reflect conduction of electrons into the solid substrate (e.g., Yanina and Rosso, 2008).

Changes in $\delta^{57}Fe/^{56}Fe$ and $\delta^{56}Fe$ values occurred over time for all experiments (Table S2). Although the initial $\delta^{56}Fe$ values for $Fe(II)_{aq}$ and goethite were similar, changes in $\delta^{56}Fe$ values demonstrate exchange of Fe isotopes, where the apparent $Fe(II)_{aq}$–goethite fractionations increased in magnitude with time (Fig. 2). As discussed above a rigorous assessment of the extent of Fe isotope exchange is provided by changes in $\delta^{57}Fe/^{56}Fe$ values, given the large initial isotopic contrast between $Fe(II)_{aq}$ and goethite, and these variations coupled with changes in $\delta^{56}Fe$ values, are illustrated in a "three-isotope" diagram in Fig. 3.

4. Discussion

Essentially 100% isotopic exchange was attained at the end of all experiments, including goethite, such that all components plotted along or close to the "secondary" mass-dependent fractionation line as dictated by the three-isotope method. As discussed below, the partial extractions identify multiple components that underwent isotopic exchange, which is interpreted to reflect different Fe(III) components, including surface Fe(III) and bulk goethite Fe(III) of different isotopic compositions. The new $Fe(II)_{aq}$–goethite fractionation factors measured here, when combined with other mineral–fluid experimental studies to obtain mineral–mineral fractionation factors, compare well with mineral–mineral Fe isotope fractionations calculated from theory, but significant differences exist between experimentally measured and calculated mineral–fluid Fe isotope fractionation factors, indicating further refinement is needed in fractionation factors calculated from theory.

4.1. Components open to Fe isotope exchange

Based on the differences in Fe isotope composition and oxidation state in the aqueous Fe and serial extractions that were measured, we

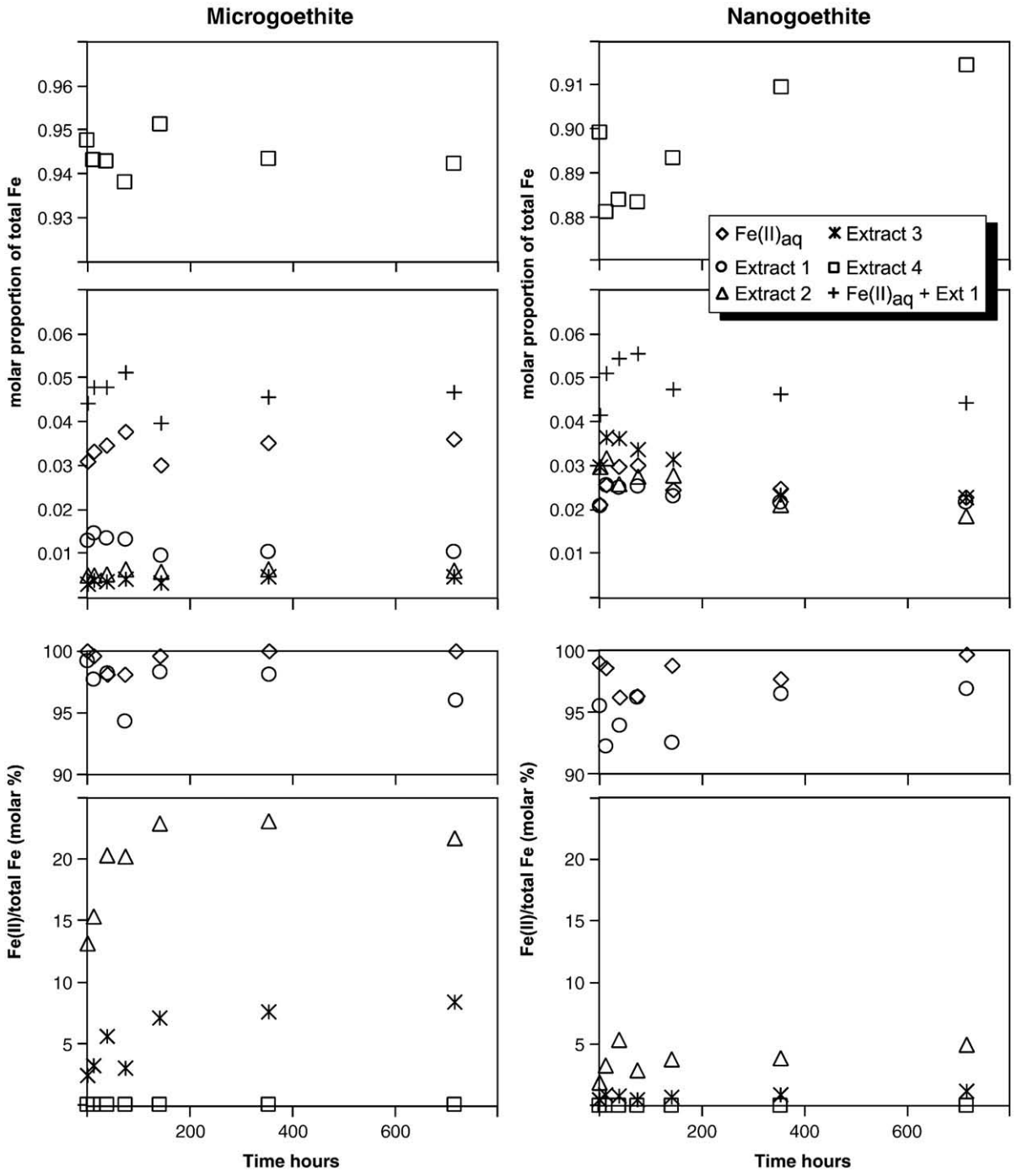

Fig. 1. Plot of molar proportion of total Fe and molar percent of Fe(II)/total Fe as a function of time that aqueous Fe(II) is allowed to equilibrate with micro and nanogoethite. Note the breaks in scale; the bulk of the total Fe is contained in the goethite (residue) fraction. Additionally, there is a break in scale for the molar percent of Fe(II) to total Fe where aqueous Fe and extract 1 are >90% Fe(II).

identify at least 4 components that experienced Fe isotope exchange. These components include $Fe(II)_{aq}$, $Fe(II)_{sorb}$, $Fe(III)_{surface}$, and bulk goethite. The $Fe(II)_{aq}$, $Fe(II)_{sorb}$ and bulk goethite components reflect nearly pure compositions in the aqueous Fe, extract 1, and extract 4 samples, respectively. The $Fe(III)_{surface}$ component may be characterized using extract 2 after minor correction for Fe(II) that reflects small extents of carryover of sorbed Fe(II). Operationally, we can calculate the end-member $Fe(III)_{surface}$ component by simple mass-balance relations, in which we assume that all the Fe(II) in extract 2 is $Fe(II)_{sorb}$ that had the Fe isotope composition measured in extract 1, and that all the Fe(III) is the surface ferric layer (e.g., Crosby et al., 2005, 2007). The Fe(II) correction is insignificant in the nanorod experiments because Fe(II) only comprises ~3.8% of the total Fe in extract 2, but this correction is more important in the microrod experiments, where Fe(II) comprises ~18.6% of the total Fe in extract 2. Typically, the Fe(II) correction increases the δ^{56}Fe value of the $Fe(III)_{surface}$ component by an average of 0.01‰ for the nanorods and 0.06‰ for the microrods relative to the measured δ^{56}Fe value of extract 2.

An important finding in the current study is the observation that the δ^{56}Fe values for the $Fe(III)_{surface}$ component, at complete or near-complete exchange (see Section 4.2), are higher than those of the bulk goethite, which implies that the Fe atom bonding environments of these components differ. It is unknown if the $Fe(III)_{surface}$ component has a uniform Fe isotope composition, or reflects a mixture of surface

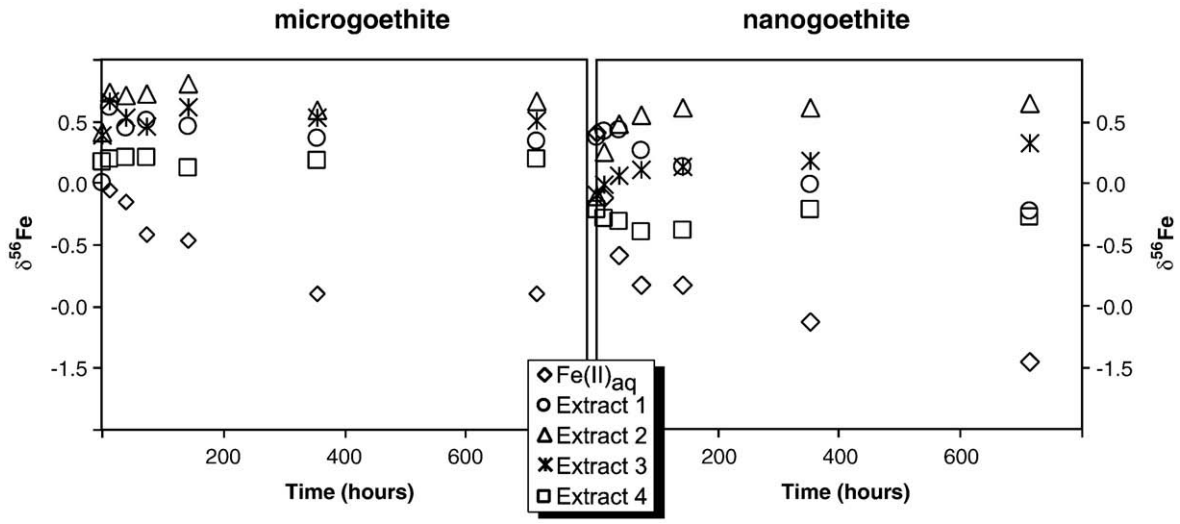

Fig. 2. Iron isotope results for the different extracts as a function of time that enriched ^{57}Fe Fe(II)$_{aq}$ is allowed to equilibrate with normal isotopic composition goethite. Data shown are for experiment A from the micro and nanogoethite experiments.

Fe and bulk goethite. If we assume that the Fe(III)$_{surface}$ component in extract 2 solely reflects surface Fe(III) that has high δ^{56}Fe values, the lower δ^{56}Fe values measured for extract 3 seem most likely to reflect a mixture of surface Fe(III) and bulk goethite. Based on a simple mixing calculation, on average, 57% of the Fe in extract 3 could be attributable to Fe(III)$_{surface}$ for both the nano and microrods, with the balance of Fe from bulk goethite. Based on these calculations, the Fe(III)$_{surface}$ component sampled in extracts 2 and 3 reflects 4.2 ± 0.7% of the total Fe in the nanorods, and 0.8 ± 0.2% of the total Fe in the microrods (average and 1-standard deviation determined from the triplicate experiments for each goethite size). Assuming a rhombohedral geometry, ~20% of the Fe atoms in the nanorods should be surface atoms, and ~4% of the Fe atoms in the microrods should be surface atoms; therefore, the Fe(III)$_{surface}$ component sampled in extracts 2 and 3 seems likely to reflect only a small proportion of the total surface Fe(III) atoms of the goethite.

4.2. Three-isotope exchange constraints on equilibrium fractionation factors

The three-isotope exchange experiments used here provide the best approach for unambiguously determining the extent of isotopic exchange, and hence the likelihood that the measured isotopic fractionations reflect equilibrium conditions. It is important to note that if all phases plot on the mass-dependent fractionation line, this demonstrates that complete exchange occurred, but it does not strictly prove that isotopic equilibrium was attained. It is possible, for example, that isotopic exchange occurred through a dissolution/re-precipitation mechanism, where dissolution and precipitation rates were rapid and hence the final isotopic compositions reflect kinetic, mass-dependent fractionation. Because steady-state conditions were reached early in our experiments, and isotopic exchange continued for the length of the experiments under conditions of unchanging Fe balances, it seems likely that any dissolution/re-precipitation occurred slowly, and we therefore interpret the data obtained at complete, or near-complete isotopic exchange to reflect equilibrium isotope fractionations.

The isotopic exchange trajectories in a three-isotope experiment with multiple exchange components may deviate from the linear relations of a two-component system if different exchange rates occur for different components in a complex system. Fig. 3 shows the results for one of the nanorod experiments for ^{54}Fe/^{56}Fe–^{57}Fe/^{56}Fe variations for the four components we have identified, and these results are typical of those obtained in all experiments. In all experiments, Fe (II)$_{aq}$ and bulk goethite (extract 4) plot on the mass-fractionation line at the end of the experiment. The four components do not, however, approach the mass-fractionation line in a linear manner, and the curvilinear trends of the four components reflect multi-component "mixing" or exchange. Because the time trends of these four-component exchange experiments are curves, as compared to straight lines in simpler two-component isotope exchange experiments (e.g., Matthews et al., 1983; Shahar et al., 2008), extrapolation to the mass-fractionation line is more difficult. We note, however, that there is little difference in the extrapolated Fe isotope compositions for Fe (II)$_{aq}$ and goethite as compared to the measured values. Because these components reached essentially 100% exchange, we use the measured Fe isotope compositions to discuss the Fe isotope fractionation factors that are calculated between the various components (Table 1).

The Fe isotope fractionations between Fe(II)$_{aq}$ and the other components are shown in Fig. 4. There is no resolvable difference in the $\Delta^{56}Fe_{Fe(II)aq-Fe(II)sorb}$ fractionation factor between the nano and microrod experiments (Table 1), and the pooled $\Delta^{56}Fe_{Fe(II)aq-Fe(II)sorb}$ average of all the experiments is -1.24 ± 0.14‰ (Table 1). The equilibrium Fe(II)$_{aq}$–Fe(II)$_{sorb}$ fractionation factor measured here is significantly different than all estimates from previous studies, which ranged from −0.3 to −3.7‰ (Icopini et al., 2004; Crosby et al., 2005, 2007; Jang et al., 2008; Mikutta et al., 2009), but we note that in none of these prior studies was attainment of isotope equilibrium rigorously demonstrated. There are, however, measurable differences in the isotopic fractionation factors for other components between the nano and microrod experiments, where the $\Delta^{56}Fe_{Fe(II)aq-goethite}$ and the $\Delta^{56}Fe_{Fe(II)aq-Fe(III)surface}$ fractionations are higher in the nanorod experiments (Fig. 4; Table 1). This difference is most pronounced for the $\Delta^{56}Fe_{Fe(II)aq-Fe(III)surface}$ fractionation factor. We suggest that these differences are largely controlled by surface area effects. Extract 2 is the best representative of the Fe(III)$_{surface}$ component, and its characteristics include a high δ^{56}Fe value relative to all other components. The origin of the high δ^{56}Fe values for the Fe(III)$_{surface}$ component is most likely due to differences in bonding of Fe at the surface of the goethite as compared to Fe that is in the interior of the goethite. Possible differences in isotopic properties could include the decrease in number of bonds to structural oxygen as compared to the interior of goethite, or energetic changes due to crystal defects, edges, or corners on the surface, or specific crystal faces. Fe(III)$_{surface}$ may reflect a variety of isotopic compositions due to these effects, as indicated by the different $\Delta^{56}Fe_{Fe(II)aq-Fe(III)surface}$ fractionations measured for the nanorod and microrod experiments (Fig. 4). We suggest that the less negative $\Delta^{56}Fe_{Fe(II)aq-Fe(III)surface}$

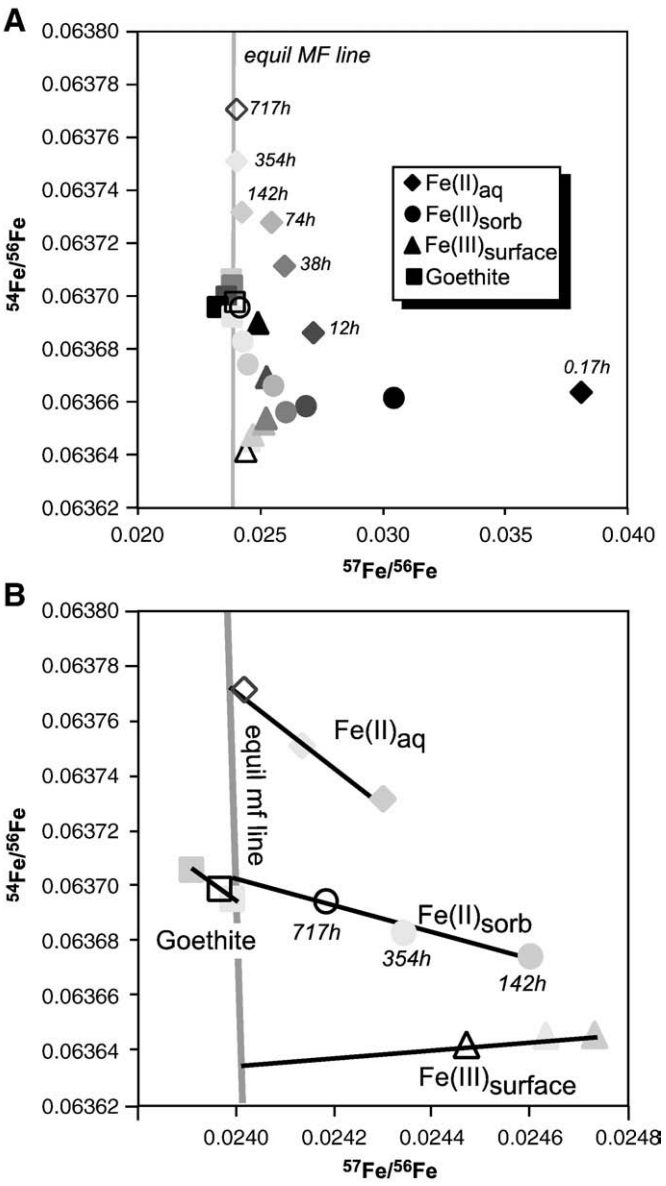

Fig. 3. Plot of $^{54}Fe/^{56}Fe$ versus $^{57}Fe/^{56}Fe$ of the different extracts. Symbols are shaded where darkest symbols represent the earliest time points. Isotope data are plotted with a common denominator such that two-component mixing will be a straight line. Because there are multiple components that formed during this experiment the extracts define curvilinear trends in panel A. Panel B shows the possible straight line extrapolation of the different extracts to the equilibrium mass-fractionation line. The plotted data are for experiment 1A and are representative of the other experiments.

fractionation factor measured for the microrod goethite is a result of a lower proportion of surface Fe that has high $\delta^{56}Fe$ values relative to bulk Fe, as compared to the nanorod experiments.

The Fe isotope effects due to differences in bonding of Fe on the surface of goethite will be most pronounced on the high surface area-to-volume nanorod experiment, and we suggest that differential surface effects may explain the small (0.2‰), but significant, difference in the measured $\Delta^{56}Fe_{Fe(II)aq-goethite}$ fractionation factor between the nanorod experiments and the microrod experiments (Fig. 4, Table 1). Because the nanorod goethite has a higher surface area relative to the microrod goethite, the slightly more negative $\Delta^{56}Fe_{Fe(II)aq-goethite}$ fractionation factor for the nanorods is interpreted to reflect the greater proportion of surface Fe that has high $\delta^{56}Fe$ values, which is consistent with the $\Delta^{56}Fe_{Fe(II)aq-Fe(III)surface}$ fractionations. Therefore, the best estimate for the equilibrium $\Delta^{56}Fe_{Fe(II)aq-goethite}$ fractionation is the microrod experiments, which have the lowest proportion of surface Fe atoms and reflect solely the intrinsic goethite Fe bonding environment.

4.3. Comparison of fractionation factors measured by experiment and calculated from theory

Experimentally determined aqueous Fe–mineral isotope fractionation factors are available for three abiologic systems: aqueous Fe(III)–hematite (Skulan et al., 2002), aqueous Fe(II)–siderite (Wiesli et al., 2004), and aqueous Fe(II)–goethite (this study). In combination with the experimentally determined aqueous Fe(II)–Fe(III) fractionations of Johnson et al. (2002) and Welch et al. (2003), these results may be combined to obtain a self-consistent, experiment-based mineral–mineral fractionation factors, or fluid–mineral fractionations that involve a common aqueous species, $Fe(II)_{aq}$ (Table 2). In the above experimental studies, aqueous Fe largely existed as $[Fe^{II}(H_2O)_6]^{2+}$ or $[Fe^{III}(H_2O)_6]^{3+}$; additional experimental studies investigated the effects of high chloride contents (Hill et al., 2009). To compare the experimental results with isotopic fractionations calculated from theory, the isotopic fractionation factor between phases A and B is related to the reduced partition function ratio, or "beta factor" ($\beta^{56/54}$) via:

$$10^3 \ln \alpha^{56}_{A-B} = 10^3 \ln \beta^{56/54}_{A} - 10^3 \ln \beta^{56/54}_{B} \quad (5)$$

$\beta^{56/54}$ factors have been calculated for $[Fe^{II}(H_2O)_6]^{2+}$ (Anbar et al., 2005; Domagal-Goldman and Kubicki, 2008; Ottonello and Zuccolini, 2009; Schauble et al., 2001), $[Fe^{III}(H_2O)_6]^{3+}$ (Anbar et al., 2005; Domagal-Goldman and Kubicki, 2008; Domagal-Goldman et al., 2009; Hill and Schauble, 2008; Hill et al., 2009; Ottonello and Zuccolini, 2009; Schauble et al., 2001), hematite (Blanchard et al., 2009; Polyakov and Mineev, 2000; Polyakov et al., 2007), siderite (Blanchard et al., 2009; Polyakov et al., 2007), and goethite (Polyakov and Mineev, 2000). A wide variety of computational approaches and models have been used for calculating the $\beta^{56/54}$ factors for $[Fe^{II}(H_2O)_6]^{2+}$ and $[Fe^{III}(H_2O)_6]^{3+}$, and these results vary by ~2‰ for both hexaquo Fe(II) and Fe(III) at room temperature, a significant range for Fe isotopes relative to the range measured in nature.

The experimentally determined $Fe(II)_{aq}$–goethite, $Fe(II)_{aq}$–siderite, and $Fe(III)_{aq}$–hematite Fe isotope fractionation factors are consistently lower than those predicted from theory (Fig. 5). Although the calculated fluid–mineral fractionations vary by ~2‰, reflecting the wide variety of computational and modeling approaches used, there appears to be a consistent offset between calculated and experimentally measured fractionation factors. In terms of experimental studies, we have a high degree of confidence that the $Fe(II)_{aq}$–goethite fractionation factor measured in the current study reflects equilibrium conditions, because ^{57}Fe-enriched Fe was used to establish complete or near-complete isotopic exchange. Skulan et al. (2002) also used ^{57}Fe-enriched Fe to establish that, in their experiments, ~85% isotopic exchange occurred for one experiment that was representative of conditions used for several experiments that involved various dissolution/re-precipitation rates; corrections used by Skulan et al. (2002) to account for the lack of complete isotopic exchange, as well as the effects of variable dissolution/re-precipitation rates are on the order of 0.3‰ in $^{56}Fe/^{54}Fe$, which is insufficient to explain the difference between the predicted and experimentally determined $Fe(III)_{aq}$–hematite Fe isotope fractionation factor. There is no evidence that the kinetic Fe isotope fractionation factor measured by Skulan et al. (2002) may somehow be the equilibrium fractionation, as suggested by Anbar et al. (2005), a suggestion that is inconsistent with the evidence for slow isotopic exchange rates of the experiments, nor the correlation between isotopic fractionation and dissolution/re-precipitation rates. The $Fe(II)_{aq}$–siderite fractionation determined by Wiesli et al. (2004) involved the classical approach of slow precipitation; although this approach is the same as

Table 1
Fe isotope composition of Fe components at equilibrium.

Experiment	$Fe(II)_{aq}$	Goethite	$Fe(II)_{sorb}$	$Fe(III)_{surface}$	$\Delta^{56}Fe_{Fe(II)aq-goethite}$	$\Delta^{56}Fe_{Fe(II)aq-Fe(II)sorb}$	$\Delta^{56}Fe_{Fe(II)aq-Fe(III)surface}$
	$\delta^{56}Fe$	$\delta^{56}Fe$	$\delta^{56}Fe$	$\delta^{56}Fe$			
Extrapolated values using last three-times points[a]							
Nanorod A	−1.40	−0.17	−0.31	0.77	−1.23	−1.09	−2.17
Nanorod B	−1.51	−0.25	−0.37	0.86	−1.26	−1.14	−2.37
Nanorod C	−1.29	−0.11	−0.51	0.69	−1.19	−0.78	−1.99
Microrod A	−0.72	0.20	0.39	0.89	−0.92	−1.11	−1.62
Microrod B	−1.21	0.24	0.51	0.86	−1.45	−1.72	−2.07
Microrod C	−0.96	0.05	0.32	0.79	−1.01	−1.28	−1.75
Measured values of final time point (corrected for ^{57}Fe tracer)[b]							
Nanorod A	−1.46	−0.28	−0.23	0.67	−1.18	−1.23	−2.13
Nanorod B	−1.53	−0.28	−0.16	0.75	−1.25	−1.37	−2.28
Nanorod C	−1.39	−0.17	−0.39	0.51	−1.22	−1.00	−1.90
Microrod A	−0.90	0.20	0.34	0.73	−1.10	−1.24	−1.63
Microrod B	−0.90	0.12	0.41	0.84	−1.02	−1.31	−1.74
Microrod C	−0.96	0.08	0.35	0.73	−1.04	−1.31	−1.69
Weighted Average using preferred values for microrods[c]					−1.05 ± 0.08	−1.29 ± 0.08	−1.68 ± 0.08
Weighted Average using preferred values for nanorods[c]					−1.22 ± 0.08	−1.20 ± 0.46	−2.10 ± 0.48
Weighted Average using preferred values all experiments[c]					−1.13 ± 0.10	−1.24 ± 0.14	−1.89 ± 0.27

[a] Extrapolated Fe isotope compositions are based on using a straight line best fit to the final three time points for each component, to the mass-balance determined "secondary" mass-fractionation line (except for the goethite microrod C experiment which was not analyzed for the 354 hour time point). The average mass-balance "secondary" mass-fractionation line was calculated using the measured Fe isotope composition and total Fe measured in the serial extracts for all of the micro or nanorod experiments.

[b] The final measured values are "spike-subtracted" for small differences in the amount of ^{57}Fe tracer in each of the aliquots. The correction is based on using the measured $^{57}Fe/^{56}Fe$ ratio to calculate the molar ratio of normal isotope composition to spike isotope composition and using this molar ratio to subtract the small differences in $^{56}Fe/^{54}Fe$ of the enriched ^{57}Fe tracer as compared to the goethite compositions. These corrections are small, and result in a an average decrease in the Fe(II)aq and goethite $\delta^{56}Fe$ values of 0.07 and 0.02‰, respectively, relative to the measured isotopic composition.

[c] The average fractionation factor is calculated using IsoPlot (version 2.49) using a weighted average assuming that there is a 0.14‰ 2σ error for the fractionation factor which is based on the external 2 standard deviation error of 0.1‰ for an analysis and assuming the error of the fractionation factor is the square root of the sum of the square of the errors. The errors for these preferred weighted average fractionation factors are the 95% confidence interval errors calculated by IsoPlot. The Fe(II)aq isotope compositions is the aqueous Fe isotope composition of the serial extraction, the Fe(II)sorb value is extract 1, the goethite is extract 4, and the Fe(III)surface is based on extraction 2 with a subtraction for the sorbed component as discussed in text.

that accepted for C and O isotope fractionation studies, there is no rigorous proof that isotopic equilibrium is attained in such approaches, although it is certainly possible that the fractionation reflected equilibrium conditions.

Generally closer agreement between experimentally measured and calculated fractionation factors occurs if fluid–fluid and mineral–mineral fractionation factors are compared (Fig. 6). The $Fe(II)_{aq}$–$Fe(III)_{aq}$ fractionation factors measured by Johnson et al. (2002) and Welch et al. (2003) lie within 0.6‰ of the DFT-PCM and DFT models of Anbar et al. (2005), the *in vacuo* and IEFPCM models of Domagal-Goldman and Kubicki (2008), and the B3LYP (gas) model of Ottonello and Zuccolini (2009); there is a large, discrepancy, however, between experiments and the PCM-HF-UAHF (solute) model of Ottonello and Zuccolini (2009). There is excellent agreement between the experimentally determined hematite–goethite fractionation factor obtained by combining the experiments of Skulan et al. (2002), Welch et al. (2003), and the current study, with the calculated fractionations factors obtained using the $\beta^{56/54}$ factor for hematite from Polyakov et

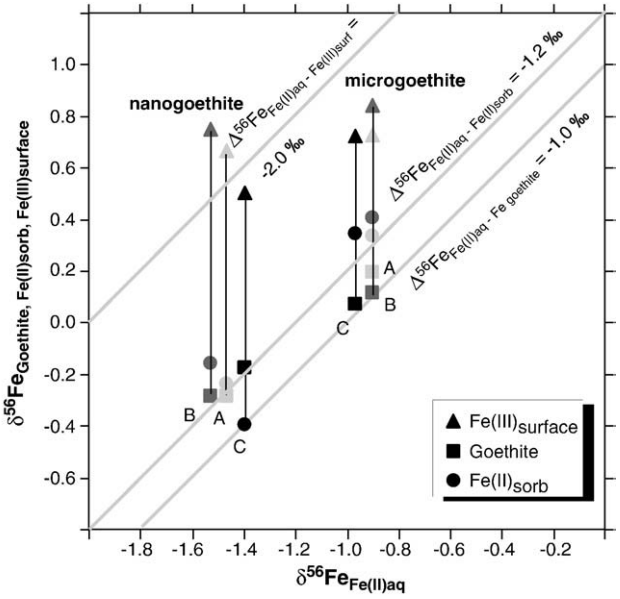

Fig. 4. Plot of the $\delta^{56}Fe$ values of the different extracts after 717 h of equilibration between $Fe(II)_{aq}$ and goethite from the micro and nanogoethite experiments. The *x*-axis is the $Fe(II)_{aq}$ and the *y*-axis is either $Fe(III)_{surface}$, bulk goethite, or $Fe(II)_{sorb}$ (see Table 1 and text for discussion of corrections). The thick grey lines show fractionation factors between $Fe(II)_{aq}$ and the other *y*-axis components.

Table 2
Experimentally determined Fe isotope fractionation factors at 20 °C in the system $Fe(II)_{aq}$–$Fe(III)_{aq}$–goethite–hematite–siderite.

	$\Delta^{56}Fe$	Notes
Fe(II)–Fe(III)	−3.01	Measured from Welch et al. (2003) and Johnson et al (2002)
Fe(II)–goethite	−1.05	This study
Fe(II)–hematite	−3.16	Calculated by combining Skulan et al. (2002) and Welch et al. (2003)[a]
Fe(II)–siderite	0.48	Measured from Wiesli et al. (2004)
Siderite–goethite	−1.53	Calculated by combining Wiesli et al. (2004) and this study
Hematite–goethite	2.11	Calculated combining Welch et al. (2003), Skulan et al. (2002), and this study[a]

There are variations in Fe isotope fractionations depending on aqueous Fe speciation (see, for example, discussion in Hill and Schauble, 2008). The above experimentally determined fractionation factors are best suited for the $Fe^{III}(H_2O)_6^{+3}$ and $Fe^{II}(H_2O)_6^{+2}$ Fe complexes; the fractionation between Fe(II) and Fe(III) will decrease by 0.2‰ per mole or chloride (Hill and Schauble, 2008). Under most geologic conditions these experimentally measured fractionations can be used without correction for aqueous Fe speciation; under unusual chloride concentrations such as oil field brines it may be necessary to apply a correction for speciation.

[a] The $\Delta^{56}Fe_{Fe(II)aq-hematite}$ is based on combining the work of Welch et al. (2003) and the Skulan et al. (2002) $\Delta^{56}Fe_{Fe(III)-hematite}$ fractionation extrapolated to a temperature of 20 °C equal to −0.15‰. This extrapolation was done assuming Arrhenius behavior on a plot of $\Delta^{56}Fe_{Fe(II)aq-hematite}$ and $10^6/T^2$, that $\Delta^{56}Fe_{Fe(II)aq-hematite} = 0$ at 10,000 °C, and the measured fractionation at 100 °C by Skulan et al. (2002) of −0.10‰.

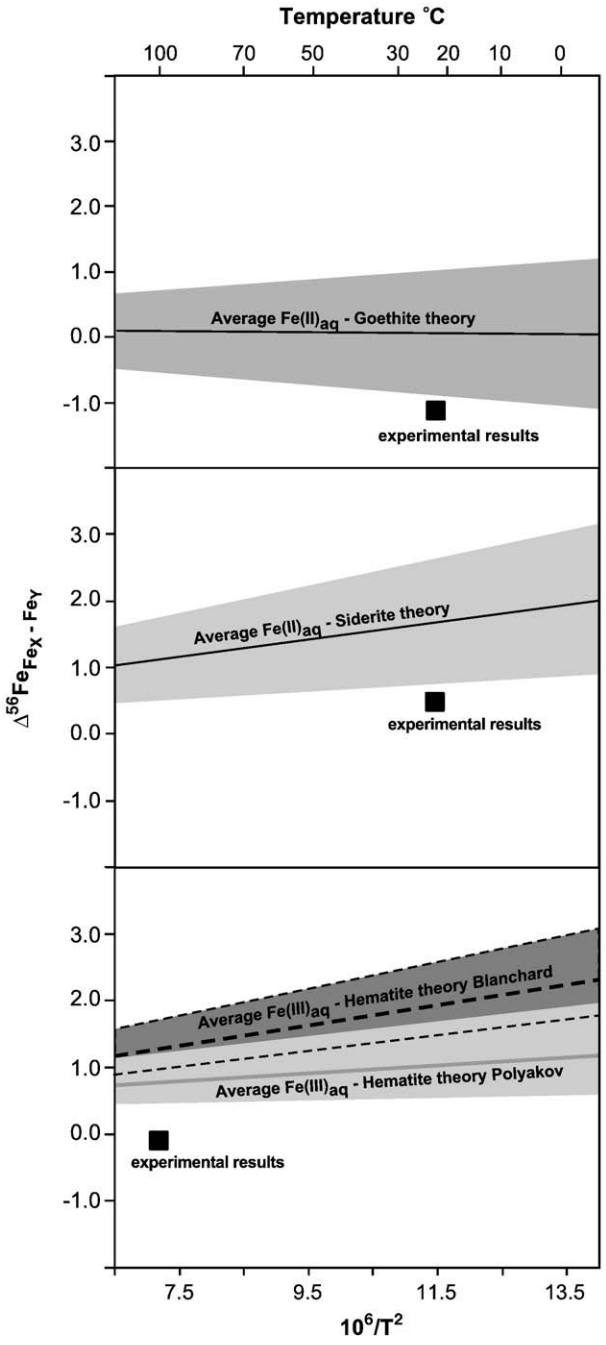

Fig. 5. Plots of aqueous Fe–mineral Fe isotope fractionations measured by experiment and combining beta values from different theoretical calculations. There is only one beta value determination for goethite (Polyakov and Mineev, 2000); two determinations for siderite (Blanchard et al., 2009; Polyakov and Mineev, 2000) which are nearly identical, and two determinations for hematite one by Polyakov et al. (2007) (labeled as Polyakov; light grey field) and the other by Blanchard et al (2009) (labeled as Blanchard; dark grey field with dotted lines). The beta values determined for $Fe^{II}(H_2O)_6^{+2}$ include values by Schauble et al. (2001); Anbar et al. (2005); Domagal-Goldman and Kubicki (2008), and Ottonello and Zuccolini (2009) and $Fe^{III}(H_2O)_6^{+3}$ beta values are from Anbar et al. (2005); Domagal-Goldman and Kubicki (2008); Hill and Schauble (2008) and Ottonello and Zuccolini (2009). The fields shown in the figure include the maximum and minimum beta values for the aqueous ferrous and ferric iron and the average of the numerical mean of the aqueous Fe beta values. The experimental results are from this study for Fe(II)–goethite, Wiesli et al. (2004) for Fe(II)–siderite, and Skulan et al. (2002) for Fe(III)–hematite.

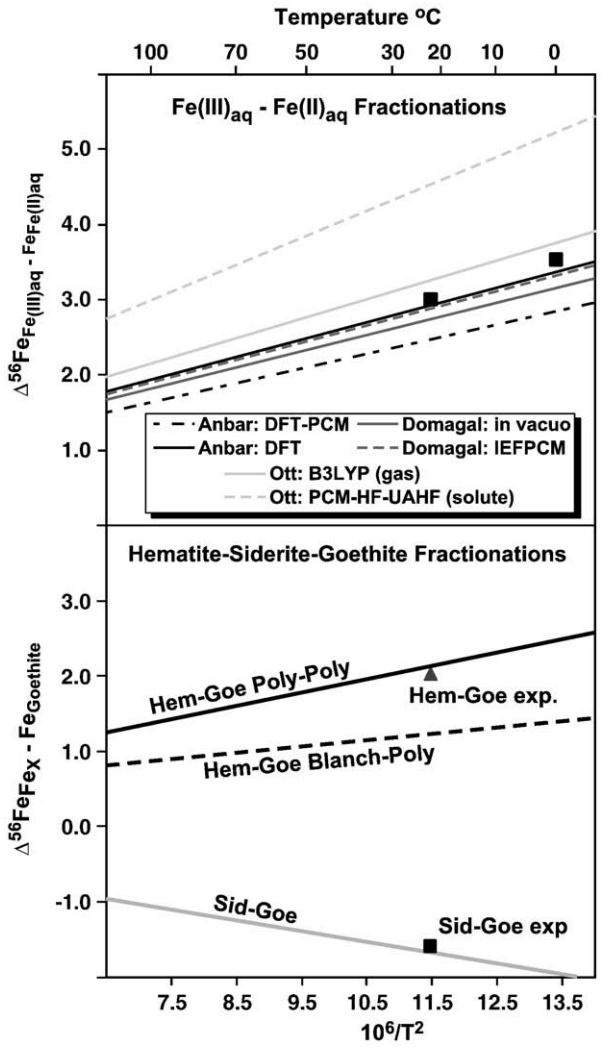

Fig. 6. Plot comparing experimentally determined siderite–goethite–hematite–Fe $(II)_{aq}$–$Fe(III)_{aq}$ fractionation factors to theoretically calculated fractionation factors ($\Delta^{56}Fe_{x-y}$) versus $10^6/T^2$. All experimentally determined fractionation factors are from experiments conducted at the University of Wisconsin Radiogenic Isotope Laboratory and the methods used for their determination are discussed in Table 2. The curves for the theoretically calculated fractionation factors for $Fe(II)_{aq}$ and $Fe(III)_{aq}$ are from different calculation methods presented by Anbar et al. (2005), Domagal-Goldman and Kubicki (2008), and Ottonello and Zuccolini (2009) and only combine beta values for the ferric and ferrous species using the same methods, which from largest to smallest $\Delta^{56}Fe_{Fe(III)-Fe(II)}$ values are, Ottonello and Zuccolini (2009) PCM-HF-UAHF (solute) and B3LYP (gas) formulations, the Anbar et al. (2005) DFT formulation, the Domagal-Goldman and Kubicki (2008) IEFPCM and in vacuo formulations, and the Anbar et al. (2005) DFT-PCM calculation. The Schauble et al. (2001) calculation is not considered because the Fe(III) beta value is a significant outlier and is suspect because of spectroscopic data issues. If all the beta values for the $Fe^{III}(H_2O)_6^{+3}$ species are considered (Anbar et al., 2005; Domagal-Goldman and Kubicki, 2008; Hill and Schauble, 2008; Ottonello and Zuccolini, 2009) there is a 1.3‰ range at 20 °C, and if all the $Fe^{II}(H_2O)_6^{+2}$ beta values are considered (Anbar et al., 2005; Domagal-Goldman and Kubicki, 2008; Ottonello and Zuccolini, 2009; Schauble et al., 2001) there is a 1.9‰ range at 20 °C. If one considered all possible formulations this could result in a $\Delta^{56}Fe_{Fe(III)-Fe(II)}$ from 1.5 to 4.7‰ at 20 °C. The theoretical calculations for the siderite–goethite fractionation uses the goethite beta value of Polyakov and Mineev (2000) and the siderite beta values of Polyakov and Mineev (2000) and Blanchard et al. (2009) which are nearly identical and agree well with the experimental results. Two curves are shown for the hematite–goethite fractionation and include the curve labeled Poly–Poly uses the Polyakov and Mineev (2000) beta value for goethite and the Polyakov et al. (2007) value for hematite and agrees well with the experimental results. The curve labeled Blanch–Poly uses the Blanchard et al. (2009) hematite beta value and the Polyakov and Mineev (2000) beta value for goethite.

al. (2007) and $\beta^{56/54}$ for goethite from Polyakov and Mineev (2000). If, however, the $\beta^{56/54}$ factor for hematite from Blanchard et al. (2009) is used, there is a 0.8‰ discrepancy between experiment and theory for the hematite–goethite fractionation factor. The experimentally determined fractionation factor for siderite–goethite obtained by combining the experiments of Wiesli et al. (2004) with the current study is identical to those calculated from theory using any combination of $\beta^{56/54}$ factors from Polyakov and Mineev (2000) and Blanchard et al.

(2009). We conclude that, on balance, the predicted $\beta^{56/54}$ factors are reliable for calculating fluid–fluid or mineral–mineral fractionations, but that it is not yet possible to confidently combine $\beta^{56/54}$ factors to calculate fluid–mineral fractionations. It is important to reconcile these inconsistencies if the Fe isotope system is to be broadly applied. Moreover, a self-consistent data set of $\beta^{56/54}$ factors that agree with experimental measurements at a single temperature will allow us to more rigorously investigate temperature sensitivity over a wide range, an approach that has been done for O isotopes (e.g., Clayton and Kieffer, 1991).

4.4. Implications for natural systems

The common occurrence of nanoparticulate goethite in lacustrine and marine sediments in part reflects the relatively low surface enthalpy for nanogoethite relative to other iron oxides (Mazeina and Navrotsky, 2005), which in turn suggests that the Fe isotope fractionations between $Fe(II)_{aq}$ and goethite may be in part controlled by surface Fe(III) rather than the bulk goethite. In their study of bacterial dissimilatory iron reduction (DIR) of goethite, Crosby et al. (2007) estimated the Fe isotope fractionation between $Fe(II)_{aq}$ and surface Fe(III) (which they termed "$Fe(III)_{reac}$") to be -2.62 ± 0.57‰, which is significantly larger in magnitude than the equilibrium Fe $(II)_{aq}$–goethite fractionation of -1.05 ± 0.08‰ measured here, but similar to the $Fe(II)_{aq}$–$Fe(III)_{surface}$ fractionation measured in the current study. The low δ^{56}Fe values that are often measured for sediment pore fluids or in lacustrine systems that have been interpreted to reflect DIR (Bergquist and Boyle, 2006; Homoky et al., 2009; Severmann et al., 2006; Tangalos et al., 2010; Teutsch et al., 2009) would be difficult to explain using the equilibrium $Fe(II)_{aq}$–goethite fractionation factor, but are more easily produced if the Fe $(II)_{aq}$–$Fe(III)_{surface}$ fractionation measured here was appropriate. This is particularly true for studies where reactive Fe(III) in the sediment has been shown to be comprised of nano crystalline goethite (e.g., Tangalos et al., 2010).

The ease with which Fe isotopes exchange via redox cycling between $Fe(II)_{aq}$ and goethite bears on the application of Fe isotopes for tracing abiologic and biologic processes in nature. For example, oxidation of Fe $(II)_{aq}$, followed by precipitation of ferric oxide/hydroxides by abiologic interaction with O_2 (e.g., Bullen et al., 2001) or through chemolithotrophic or photosynthetic Fe(II) oxidation (e.g., Balci et al., 2006; Croal et al., 2004) has been modeled as a Rayleigh process, where relatively large $Fe(II)_{aq}$–ferric oxide/hydroxide fractionations are predicted at high extents of oxidation; if isotopic re-equilibration is fairly extensive, as shown here, this would tend to decrease the apparent $Fe(II)_{aq}$–ferric oxide/hydroxide fractionations that occur toward the end of a Rayleigh process. In other systems, where pore fluid $Fe(II)_{aq}$ may interact with ferric oxide/hydroxides, the isotopic response due to exchange will depend upon the molar proportions of $Fe(II)_{aq}$ and ferric oxide/hydroxide. At low proportions of $Fe(II)_{aq}$ to ferric oxide/hydroxides, the largest shifts in Fe isotope compositions will occur in the $Fe(II)_{aq}$ component; in contrast, under conditions of extensive flow of $Fe(II)_{aq}$ through a ferric oxide/hydroxide matrix, the Fe isotope compositions of $Fe(II)_{aq}$ will initially shift but then recover to be equal to the δ^{56}Fe value of the input $Fe(II)_{aq}$ (e.g., Mikutta et al., 2009). Our results bear importantly on proposals that Fe isotopes may be an indicator of DIR in natural systems; the continued exposure of new surface atoms that occurs during DIR, and the associated relatively large magnitude Fe $(II)_{aq}$–$Fe(III)_{surface}$ fractionation determined in the current study, supports the interpretation that DIR is the most efficient process for producing large quantities of low-δ^{56}Fe $Fe(II)_{aq}$.

4.5. Implications for oxygen isotope geochemistry

The large extent of isotopic exchange obtained here during Fe redox cycling may warrant a new approach for determining equilibrium O isotope fractionation factors for oxide–water systems. Oxygen isotope compositions of authigenic iron oxides remain an important means for determining paleotemperatures and/or groundwater fluid sources (Bao et al., 2000; Yapp, 1987, 1990), and the δ^{18}O values of goethite may sufficiently resist diagenetic alteration to serve as a paleotemperature proxy (Yapp, 1998). Currently, however, a large range in $^{18}O/^{16}O$ fractionation factors exist for water-oxide systems at low temperatures, up to ~10‰ to 16‰ depending on oxide phase, posing a significant obstacle to interpreting δ^{18}O values for iron oxides from natural systems. To date, $^{18}O/^{16}O$ fractionation studies at low temperatures have relied on precipitation methods, where assessment of equilibrium conditions requires consideration of precipitation rates and solid phase conversion (Bao and Koch, 1999; Bao et al., 2000). Previous O isotope water-oxide experiments involved pure water, where limited recrystallization occurred, but our work shows that complete Fe isotope exchange may be attained between $Fe(II)_{aq}$ and iron oxides via redox cycling, and if complete Fe isotope exchange occurs, complete O isotope exchange may occur as well. The concentrations of $Fe(II)_{aq}$ required to promote complete isotopic exchange are not high, and unlikely to impart "salt effects" in stable O isotope fractionation experiments (e.g., Hu and Clayton, 2003). For example, in the experiments of the current study, the molar Fe/O ratio in the solutions was $\sim10^{-5}$, which would not produce a significant "salt effect" because the proportion of Fe–H_2O bonds, relative to H_2O–H_2O bonds, is small.

5. Conclusions

A set of three-isotope method experiments constrains the equilibrium Fe isotope fractionations among aqueous and sorbed Fe (II), surface Fe(III), and bulk goethite, where complete or near-complete isotopic exchange was achieved using both nanorod and microrod goethite at room temperature over 30 days. The fractionation between $Fe(II)_{aq}$ and $Fe(II)_{sorb}$ is -1.24‰ in $^{56}Fe/^{54}Fe$, and this value is indistinguishable in both the nano and microrod experiments. Previous experimental work on Fe isotope fractionations between Fe $(II)_{aq}$ and $Fe(II)_{sorb}$ have produced a wide range of results, but the current study is the first that clearly establishes an equilibrium fractionation factor between $Fe(II)_{aq}$ and $Fe(II)_{sorb}$ for goethite. The isotopic fractionation between surface Fe(III), as sampled by stepwise acid leaching, and $Fe(II)_{aq}$ varies from $+2.37$ to $+1.63$‰, and this is significantly different than the bulk goethite–$Fe(II)_{aq}$ fractionation. These differences are interpreted to reflect differences in Fe(III) bonding between surface Fe and Fe in bulk goethite. This observation in turn may explain the small differences in the equilibrium fractionation factor between $Fe(II)_{aq}$ and goethite measured for the nano and microrod experiments, which likely originate from the significant differences in surface area for these iron oxides. These isotope differences illustrate that nanoparticles may have distinct isotopic properties from larger crystals; because such properties are related to classical thermodynamic properties, this result is an extension of the common observation that the thermodynamic properties of nanoparticles may be distinct from those of larger crystals (e.g., Navrotsky et al., 2008). Although use of nanoparticles may be attractive in experimental studies of mass-dependent isotope fractionation factors because of increased rates of isotopic exchange relative to larger minerals, the results of this study suggest that surface area-to-volume effects may be critical. We consider the microrod experiments to be the best measurement of the equilibrium fractionation between $Fe(II)_{aq}$ and goethite because these experiments were least affected by the $Fe(III)_{surface}$ component; using the microrod experiments produces an equilibrium $Fe(II)_{aq}$–goethite fractionation of -1.05 ± 0.08‰ at 20 °C. Compared to the $Fe(II)_{aq}$–goethite fractionations calculated from theory, the experimentally determined fractionation is significantly lower, an observation seen in comparisons of $Fe(II)_{aq}$–siderite and $Fe(III)_{aq}$–hematite fractionations measured in experiment and calculated from theory. In contrast,

siderite–goethite and hematite–goethite fractionations obtained from experiments and theory generally agree, suggesting that it is not yet possible to combine predicted reduced partition coefficient ratios for fluids and minerals to obtain fluid–mineral fractionation factors.

Acknowledgements

Financial support was provided by National Science Foundation grant 0506679 and NASA grant NNG05GP35G. We thank Alan Matthews and an anonymous reviewer for helpful comments.

Appendix A. Supplementary data

Supplementary data associated with this article can be found, in the online version, at doi:10.1016/j.epsl.2010.04.006.

References

Anbar, A.D., Jarzecki, A.A., Spiro, T.G., 2005. Theoretical investigation of iron isotope fractionation between $Fe(H_2O)_6^{3+}$ and $Fe(H_2O)_6^{2+}$: implications for iron stable isotope geochemistry. Geochim. Cosmochim. Acta 69, 825–837.

Balci, N., Bullen, T.D., Witte-Lien, K., et al., 2006. Iron isotope fractionation during microbially stimulated Fe(II) oxidation and Fe(III) precipitation. Geochim. Cosmochim. Acta 70, 622–639.

Bao, H.M., Koch, P.L., 1999. Oxygen isotope fractionation in ferric oxide–water systems: low temperature synthesis. Geochim. Cosmochim. Acta 63, 599–613.

Bao, H.M., Koch, P.L., Thiemens, M.H., 2000. Oxygen isotopic composition of ferric oxides from recent soil, hydrologic, and marine environments. Geochim. Cosmochim. Acta 64, 2221–2231.

Beard, B.L., Johnson, C.M., Skulan, J.L., et al., 2003. Application of Fe isotopes to tracing the geochemical and biological cycling of Fe. Chem. Geol. 195, 87–117.

Bergquist, B.A., Boyle, E.A., 2006. Iron isotopes in the Amazon River system: weathering and transport signatures. Earth Planet. Sci. Lett. 248, 54–68.

Blanchard, M., Poitrasson, F., Méheut, M., et al., 2009. Iron isotope fractionation between pyrite (FeS_2), hematite (Fe_2O_3) and siderite ($FeCO_3$): a first-principles density functional theory study. Geochim. Cosmochim. Acta 73, 6565–6578.

Bullen, T.D., White, A.F., Childs, C.W., Vivit, D.V., Schulz, M.S., 2001. Demonstration of significant abiotic iron isotope fractionation in nature. Geology 29, 699–702.

Clayton, R.N., Kieffer, S.W., 1991. Oxygen isotopic thermometer calibrations. In: Taylor, H.P., O'Neil Jr., J.R., Kaplan, I.R. (Eds.), Stable Isotope Geochemistry; Attributed to Samuel Epstein Special Publication — Geochemical Society. Geochemical Society, University Park, Pa, pp. 3–10.

Croal, L.R., Johnson, C.M., Beard, B.L., Newman, D.K., 2004. Iron isotope fractionation by Fe (II)-oxidizing photoautotrophic bacteria. Geochim. Cosmochim. Acta 68, 1227–1242.

Crosby, H.A., Johnson, C.M., Roden, E.E., Beard, B.L., 2005. Coupled Fe(II)–Fe(III) electron and atom exchange as a mechanism for Fe isotope fractionation during dissimilatory iron oxide reduction. Environ. Sci. Technol. 39, 6698–6704.

Crosby, H.A., Roden, E.E., Johnson, C.M., Beard, B.L., 2007. The mechanisms of iron isotope fractionation produced during dissimilatory Fe(III) reduction by *Shewanella putrefaciens* and *Geobacter sulfurreducens*. Geobiology 5, 169–189.

Cwiertny, D.M., Handler, R.M., Schaefer, M.V., Grassian, V.H., Scherer, M.M., 2008. Interpreting nanoscale size-effects in aggregated Fe-oxide suspensions: reaction of Fe(II) with goethite. Geochim. Cosmochim. Acta 72, 1365–1380.

Domagal-Goldman, S.D., Kubicki, J.D., 2008. Density functional theory predictions of equilibrium isotope fractionation of iron due to redox changes and organic complexation. Geochim. Cosmochim. Acta 72, 5201–5216.

Domagal-Goldman, S.D., Paul, K.W., Sparks, D.L., Kubicki, J.D., 2009. Quantum chemical study of the Fe(III)–desferrioxamine B siderophore complex—electronic structure, vibrational frequencies, and equilibrium Fe-isotope fractionation. Geochim. Cosmochim. Acta 73, 1–12.

Gorski, C.A., Scherer, M.M., 2009. Influence of magnetite stoichiometry on Fe(II) uptake and nitrobenzene reduction. Environ. Sci. Technol. 43, 3675–3680.

Handler, R.M., Beard, B.L., Johnson, C.M., Scherer, M.M., 2009. Atom exchange between aqueous Fe(II) and goethite: an Fe isotope tracer study. Environ. Sci. Technol. 43, 1102–1107.

Hansel, C.M., Benner, S.G., Fendorf, S., 2005. Competing Fe(II)-induced mineralization pathways of ferrihydrite. Environ. Sci. Technol. 39, 7147–7153.

Hill, P.S., Schauble, E.A., 2008. Modeling the effects of bond environment on equilibrium iron isotope fractionation in ferric aquo-chloro complexes. Geochim. Cosmochim. Acta 72, 1939–1958.

Hill, P.S., Schauble, E.A., Shahar, A., Tonui, E., Young, E.D., 2009. Experimental studies of equilibrium iron isotope fractionation in ferric aquo-chloro complexes. Geochim. Cosmochim. Acta 73, 2366–2381.

Homoky, W.B., Severmann, S., Mills, R.A., Statham, P.J., Fones, G.R., 2009. Pore-fluid Fe isotopes reflect the extent of benthic Fe redox cycling: evidence from continental shelf and deep-sea sediments. Geology 37, 751–754.

Hu, G.X., Clayton, R.N., 2003. Oxygen isotope salt effects at high pressure and high temperature and the calibration of oxygen isotope geothermometers. Geochim. Cosmochim. Acta 67, 3227–3246.

Icopini, G.A., Anbar, A.D., Ruebush, S.S., Tien, M., Brantley, S.L., 2004. Iron isotope fractionation during microbial reduction of iron: the importance of adsorption. Geology 32, 205–208.

Jang, J.H., Mathur, R., Liermann, L.J., Ruebush, S., Brantley, S.L., 2008. An iron isotope signature related to electron transfer between aqueous ferrous iron and goethite. Chem. Geol. 250, 40–48.

Johnson, C.M., Skulan, J.L., Beard, B.L., et al., 2002. Isotopic fractionation between Fe(III) and Fe(II) in aqueous solutions. Earth Planet. Sci. Lett. 195, 141–153.

Larese-Casanova, P., Scherer, M.M., 2007. Fe(II) sorption on hematite: new insights based on spectroscopic measurements. Environ. Sci. Technol. 41, 471–477.

Matsuhisa, Y., Goldsmith, J.R., Clayton, R.N., 1978. Mechanisms of hydrothermal crystallization of quartz at 250 °C and 15 kbar. Geochim. Cosmochim. Acta 42, 173–182.

Matthews, A., Goldsmith, J.R., Clayton, R.N., 1983. On the mechanisms and kinetics of oxygen isotope exchange in quartz and feldspars at elevated-temperatures and pressures. Geol. Soc. Am. Bull. 94, 396–412.

Mazeina, L., Navrotsky, A., 2005. Surface enthalpy of goethite. Clays Clay Minerals 53, 113–122.

Mikutta, C., Wiederhold, J.G., Cirpka, O.A., et al., 2009. Iron isotope fractionation and atom exchange during sorption of ferrous iron to mineral surfaces. Geochim. Cosmochim. Acta 73, 1795–1812.

Navrotsky, A., Mazeina, L., Majzlan, J., 2008. Size-driven structural and thermodynamic complexity in iron oxides. Science 319, 1635–1638.

Ottonello, G., Zuccolini, M.V., 2009. Ab-initio structure, energy and stable Fe isotope equilibrium fractionation of some geochemically relevant H–O–Fe complexes. Geochim. Cosmochim. Acta 73, 6447–6469.

Pedersen, H.D., Postma, D., Jakobsen, R., Larsen, O., 2005. Fast transformation of iron oxyhydroxides by the catalytic action of aqueous Fe(II). Geochim. Cosmochim. Acta 69, 3967–3977.

Polyakov, V.B., Mineev, S.D., 2000. The use of Mossbauer spectroscopy in stable isotope geochemistry. Geochim. Cosmochim. Acta 64, 849–865.

Polyakov, V.B., Clayton, R.N., Horita, J., Mineev, S.D., 2007. Equilibrium iron isotope fractionation factors of minerals: reevaluation from the data of nuclear inelastic resonant X-ray scattering and Mossbauer spectroscopy. Geochim. Cosmochim. Acta 71, 3833–3846.

Schauble, E.A., Rossman, G.R., Taylor, H.P., 2001. Theoretical estimates of equilibrium Fe-isotope fractionations from vibrational spectroscopy. Geochim. Cosmochim. Acta 65, 2487–2497.

Severmann, S., Johnson, C.M., Beard, B.L., McManus, J., 2006. The effect of early diagenesis on the Fe isotope compositions of porewaters and authigenic minerals in continental margin sediments. Geochim. Cosmochim. Acta 70, 2006–2022.

Shahar, A., Young, E.D., Manning, C.E., 2008. Equilibrium high-temperature Fe isotope fractionation between fayalite and magnetite: an experimental calibration. Earth Planet. Sci. Lett. 268, 330–338.

Silvester, E., Charlet, L., Tournassat, C., et al., 2005. Redox potential measurements and Mossbauer spectrometry of Fe-II adsorbed onto Fe-III (oxyhydr)oxides. Geochim. Cosmochim. Acta 69, 4801–4815.

Skulan, J.L., Beard, B.L., Johnson, C.M., 2002. Kinetic and equilibrium Fe isotope fractionation between aqueous Fe(III) and hematite. Geochim. Cosmochim. Acta 66, 2995–3015.

Tangalos, G.E., Beard, B.L., Johnson, C.M., et al., 2010. Microbial production of isotopically light iron(II) in a modern chemically precipitated sediment and implications for isotopic variations in ancient rocks. Geobiology 8, 197–208.

Teutsch, N., Schmid, M., Müller, B., et al., 2009. Large iron isotope fractionation at the oxic–anoxic boundary in Lake Nyos. Earth Planet. Sci. Lett. 285, 52–60.

van der Zee, C., Roberts, D.R., Rancourt, D.G., Slomp, C.P., 2003. Nanogoethite is the dominant reactive oxyhydroxide phase in lake and marine sediments. Geology 31, 993–996.

Welch, S.A., Beard, B.L., Johnson, C.M., Braterman, P.S., 2003. Equilibrium Fe isotope fractionation between ferrous and ferric iron. Geochim. Cosmochim. Acta 67, A529.

Wiesli, R.A., Beard, B.L., Johnson, C.M., 2004. Experimental determination of Fe isotope fractionation between aqueous Fe(II), siderite and "green rust" in abiotic systems. Chem. Geol. 211, 343–362.

Williams, A.G.B., Scherer, M.M., 2004. Spectroscopic evidence for Fe(II)–Fe(III) electron transfer at the iron oxide–water interface. Environ. Sci. Technol. 38, 4782–4790.

Yanina, S.V., Rosso, K.M., 2008. Linked reactivity at mineral–water interfaces through bulk crystal conduction. Science 320, 218–222.

Yapp, C.J., 1987. Oxygen and hydrogen isotope variations among goethites (Alpha-FeOOH) and the determination of paleotemperatures. Geochim. Cosmochim. Acta 51, 355–364.

Yapp, C.J., 1990. Oxygen isotopes in iron (III) oxides. 1. Mineral–water fractionation factors. Chem. Geol. 85, 329–335.

Yapp, C.J., 1998. Paleoenvironmental interpretations of oxygen isotope ratios in oolitic ironstones. Geochim. Cosmochim. Acta 62, 2409–2420.